



HAL
open science

Hydrotreatment of Sewage Sludge Derived Hydrothermal Liquefaction Biocrude. Part II: Kinetic Model

Barbara Browning, Nuno Batalha, Nouredine Lebaz, Christophe Geantet,
Melaz Tayakout-Fayolle

► **To cite this version:**

Barbara Browning, Nuno Batalha, Nouredine Lebaz, Christophe Geantet, Melaz Tayakout-Fayolle. Hydrotreatment of Sewage Sludge Derived Hydrothermal Liquefaction Biocrude. Part II: Kinetic Model. *Energy & Fuels*, 2024, 38 (13), pp.11805-11814. 10.1021/acs.energyfuels.4c00901 . hal-04658121

HAL Id: hal-04658121

<https://hal.science/hal-04658121v1>

Submitted on 22 Jul 2024

HAL is a multi-disciplinary open access archive for the deposit and dissemination of scientific research documents, whether they are published or not. The documents may come from teaching and research institutions in France or abroad, or from public or private research centers.

L'archive ouverte pluridisciplinaire **HAL**, est destinée au dépôt et à la diffusion de documents scientifiques de niveau recherche, publiés ou non, émanant des établissements d'enseignement et de recherche français ou étrangers, des laboratoires publics ou privés.

Hydrotreatment of Sewage Sludge Derived Hydrothermal Liquefaction Biocrude. Part II: Kinetic Model

Barbara Browning^{a}, Nuno Rocha Batalha^b, Nouredine Lebaz^a, Christophe Geantet^b, Melaz Tayakout-Fayolle^a.*

^a Univ Lyon, Université Claude Bernard Lyon 1, CNRS, LAGEPP UMR 5007, 43 Boulevard du 11 novembre 1918, F-69100, Villeurbanne, France

^b Univ Lyon, Université Claude Bernard Lyon 1, CNRS, IRCELYON UMR 5256, 2 Avenue Albert Einstein, F-69626, Villeurbanne, France

KEYWORDS: Sewage sludge, Hydrothermal Liquefaction, Hydrotreatment, Distributed kinetic model, Parameter estimation, Carbon numbers

ABSTRACT:

A kinetic model comprising 11 component families, 153 distributed lumps and 117 first-order reactions was constructed to represent the hydrotreatment of a sewage sludge-derived HTL biocrude. The model was based on 15 laboratory-scale experiments with biocrude solubilised in

heptane in a batch reactor and contacted with a hydrotreatment catalyst under 100 bars of hydrogen. Experiments were of duration 0 – 5h and performed at 350, 375 and 390°C. The mass balance was closed to at least 87% and reactor outputs were analysed with reaction liquids quantified by structure and carbon number in the form of mass distributions. A reaction scheme with three sections: straight chains, aromatics and heavy lumps was proposed. 26 kinetic parameters were estimated, all significant to more than 95%. Model outputs compare well with measured data.

1. Introduction

Hydrothermal Liquefaction (HTL) has the potential to turn organic waste streams into useful liquid fuels¹. It produces high-viscosity biocrudes with high heteroatom content which require further upgrading^{2,3}. Several studies characterised sewage sludge-derived biocrudes in detail: Fan et al. (2022) reviewed HTL and upgrading of sewage sludge for biofuels⁴, Zimmermann et al. (2022) confirmed the presence of long-chain fatty acids and amides⁵ and Jahromi et al. (2022) demonstrated the consequence of HTL solvent type on biocrude hydrotreatment⁶. Sewage sludge-derived biocrudes vary according to HTL processing method, the type of sewage sludge source and with geography⁴⁻⁷.

Hydrotreatment is a well-understood process^{8,9} and co-processing of sewage sludge-derived biocrudes with traditional heavy oil feedstocks is a possibility for upgrading on the industrial scale^{3,10,11}. Laboratory scale hydrotreatment of biocrudes has focussed on reaction conditions and feedstock and product characterisation^{2,3,7}. Batalha et al. (2023) made a detailed comprehensive analysis of several HTL biocrudes and their upgrading products² and, working with a real sewage sludge-derived biocrude, Heracleous et al. (2022) found that long chain fatty acids were easily converted into their respective paraffins, with heteroatom removal and

increased viscosity reduction at higher reaction temperature⁷. Zhu et al. (2022) used model molecules to determine kinetic parameters for hydrotreatment of long-chain amides, finding deoxygenation (DO) faster than denitrogenation (DN), with a long-chain aliphatic amine as the main intermediate¹⁰.

Zhu et al. (2022) assumed first-order kinetics in their model to compare pathways for model long chain amides conversion¹⁰. A wide range of dynamic models have been applied to hydrotreating traditional feedstocks. Compounds are usually lumped by heteroatom, e.g. the hydrodenitrogenation (HDN) reaction rate equation would apply to the total nitrogen content^{8,9}. First-order kinetics are generally used for an initial analysis and chemical complexity can be taken into account by using nth order kinetics^{8,9}. More detailed hydrotreatment models include model compounds and can use reaction rate equations based on Langmuir-Hinshelwood kinetics⁹ as N compounds are self-inhibiting for HDN¹². Pu et al. (2020) constructed a kinetic model based on GCxGC analysis of liquid products after catalytic hydroconversion of lignin and used a first-order reaction rate equation with respect to the components and hydrogen concentration¹³.

Mass distributions have been used for detailed modelling and simulation of upgrading residues and vacuum gas oils¹⁴⁻¹⁶. This method allows for mole-based reaction rate equations and a good representation of the reaction liquid physical properties¹⁴⁻¹⁶.

Browning et al. (Browning et al., 2024) in Part I have performed hydrotreatment experiments of sewage sludge-derived biocrude. All products and reagents were analysed as thoroughly as possible using the available analytical techniques. The data is the carbon number mass distributions for sewage sludge biocrude components and upgrading products (Browning et al., 2024). After a detailed mechanism analysis, several reaction networks were tested against the

data and then adjusted based on model fit and parameter estimation results. Only the best one is presented in this Part II article. For this modelling, we have used quantitative data from 15 experiments covering three temperatures (350°C, 375°C, and 390°C), and with durations up to 5 hours, to test a distributed dynamic model for hydrotreatment of a sewage sludge-derived biocrude. Parameter estimation allowed us to find the reaction constants, activation energies and stoichiometric coefficients associated with the reactions in the kinetic model.

2. Material and methods

2.1 Experimental methods

The experimental methods have been described by Browning et al. (2024)². To recap briefly, sewage sludge-derived biocrude was produced by hydrothermal liquefaction experiments in a 1000 mL batch reactor. Subsequently, hydrotreatment was performed on 3g of the biocrude with 1g of solid catalyst (NiMoS/Al₂O₃, described in Table 2 of Browning et al. (2024)²), diluted in 30g of heptane, at temperatures of 350°C, 375°C, and 390°C under 100 bars of H₂ in a 300 mL batch reactor. As soon as the experimental temperature was reached, the hydrogen charge was completed and the reaction time, t_0 , was set. The reactor was cooled rapidly at the end of the reaction period. The resulting reaction products included liquid, gas, solids, and dissolved gases. Liquid products were separated from heptane through evaporation in a rotary evaporator for 2 hours at 30 mbar and 40°C. A mass balance was conducted, with losses primarily observed in experiments of longer duration (5 hours), achieving at least 83% closure. Gas components were analyzed using micro-Gas Chromatography (SRA instruments), with a portion remaining dissolved in the liquid heptane at cold reactor conditions. Missing mass quantities were calculated using a process simulator

(ProSimPlus™) based on measured gas phase composition, assuming equilibrium between gas and liquid phases, resulting in mass balance closure between 87% and 97%. Elemental analysis of liquid and solid products was performed using a Thermo Scientific Flash 2000 Organic Elemental Analyser². Liquid product identification and quantification were conducted using comprehensive two-dimensional mass spectrometry, time of flight mass spectrometry, and flame ionisation detector gas chromatography (GCxGC – MS, GCxGC – TOFMS, and GCxGC – FID)². The component families were classified as: amides, nitriles, aliphatic amines, aliphatics, indoles, carbazoles, phenols, N-aromatics, O- N-aromatics, pyridines, diaromatics and monoaromatics. Liquid product analyses were transformed into carbon number distributions using Simulated Distillation (SimDis ASTM 2887) analysis and Size Exclusion Chromatography (SEC)². The carbon number distributions were adjusted to account for additional nitrogen and oxygen, where necessary, and were normalized to the initial biocrude mass charge of the 350°C, t₀ experiment.

3. Model construction

After careful review, results from 15 experiments were retained for modelling as shown in Table 1: a t₀ experiment for each reaction temperature plus reactions of duration 0.5, 1 and 5 h at 350°C, 0.5, 1, 3 and 5 h at 375 and 390°C and one repeat 3h experiment at 375°C. For each experiment, there were 164 data points including 153 distributed lumps across the eleven families. All data points are used for parameter estimation. Modelling the upgrading reaction kinetics was an iterative process. After a detailed mechanism analysis, several reaction networks were tested against the data and then adjusted based on model fit and parameter estimation results. Only the best one is presented in this article.

Temperature (°C)	Duration (h)
------------------	--------------

350	0, 0.5, 1, 5
375	0, 0.5, 1, 3, 3 (repeat), 5
390	0, 0.5, 1, 3, 5

Table 1. List of experiments

3.1 Reactor Model

Experiments were performed in an agitated batch reactor and the reaction mixture was diluted by a factor of ten in supercritical heptane under reaction conditions, known to facilitate mass transfer of H₂ to the catalyst¹⁷⁻¹⁹. We therefore assume a single homogeneous phase and no mass transfer limitation, either intraparticle or at the catalyst boundary.

Molar masses have been calculated for all components including distributed lumps and the reaction model is constructed on a molar basis. Molar quantities are converted back into mass for parameter estimation. The distributed masses for each family can be summed to give the total and represent its overall evolution. The mole balances are given by Eq. (1), where $V_R(m^3)$ is the reactor volume and $r_{f,i}(mol.h^{-1})$ the reaction rate for component, i , in family, f . Components can be consumed or produced by more than one reaction. $C_j(mol.m^{-3})$ is the concentration of component, j , and $\gamma_{j,f,i}$ is the stoichiometric coefficient relating components i and j . NR and NF are the total number of reactions and families where j is produced or consumed.

$V_R \frac{dC_j}{dt} = r_j = \sum_{f=1}^{NF} \sum_{i=1}^{NR} \gamma_{j,f,i} r_{f,i}$	(1)
--	-----

The eleven component families, f , are: amides, nitriles, aliphatic amines, aliphatics, carbazoles, phenols, N-aromatics, O- N-aromatics, pyridines, diaromatics and monoaromatics. Additional components are H_2 , H_2O , NH_3 , CH_4 , C_2H_6 , solid CHO, solid N and losses.

3.2 Kinetic model

The optimised reaction scheme is presented in Figure 1 and has three distinct groups: straight chains, aromatics and heavy (C_{30+}) and solid lumps. All the species shown in Figure 1 (a) and (b) are carbon number distributions, whereas the C_{30+} and solid in Figure 1 (c) are combined lumps. Various reaction schemes were tested, including reactions where the straight chain and aromatics families were interconnected. However, potential reactions linking the straight chains to the aromatics were not found to be significant. Reactions and reaction rate equations are listed in

Table 2 where $k_r(m^3 \cdot mol^{-1} \cdot h^{-1})$ is the overall reaction rate constant for reaction r . k_r , defined with respect to reference temperature ($T_{ref} = 350^\circ C$), can be written as follows:

$$k_r = k_{r,T_{ref}} e^{-\frac{Ea_r}{R} \left(\frac{1}{T} - \frac{1}{T_{ref}} \right)} \quad (2)$$

T (K) is the experimental temperature, $k_{r,T_{ref}}(m^3 \cdot mol^{-1} \cdot h^{-1})$ is the preexponential factor of k_r at the reference temperature T_{ref} , $Ea_r(kJ \cdot mol^{-1})$ is the activation energy for reaction r and $R(kJ \cdot mol^{-1} \cdot K^{-1})$ is the ideal gas constant. The component family names are shortened as follows: amides (Ad), nitriles (Nt), aliphatic amines (An), aliphatics (Al), carbazoles (Cb), phenols (Ph), N-aromatics (Rn), O- N-aromatics (Ro), pyridines (Pp), diaromatics (Da), monoaromatics (Ma) and losses (L).

Table 2 also includes the carbon number range for each reaction. All reactions consume H_2 and are considered first-order with respect to the concentrations of the reacting component and H_2 . Activation energies were initially estimated for all reactions but only significant results were kept. Some stoichiometric coefficients are fixed parameters and some are for estimation.

The straight chain reactions are separated into two groups as shown in Figure 1 (a), C15 – C19 and C20 – C29. For reactions 1 and 2, only the functional groups react, carbon numbers remain unchanged. Amides and nitriles produce aliphatic amines, with amides also producing H_2O in reaction 1. In reaction 3, aliphatic amines produce aliphatics and NH_3 . Carbon numbers C15 to C19 remain unchanged, whilst heavier C20 to C29 compounds break into two halves. The straight chain reactions are all well-defined and the stoichiometric coefficients are as follows:

$\gamma_{H_2,Ad,i} = 2$, $\gamma_{H_2,Nt,i} = 2$ and $\gamma_{H_2,An,i} = 1$ for C15 – C19 and 2 for C20 – C29.

Figure 1 (b) illustrates the aromatics carbon number distribution reactions, reaction numbers 4 – 9. Despite being identified in the reaction mixture, indoles are not included in the model because of the earlier assumption that they don't react. The monoaromatics are produced in reactions 4 – 6 from C9+ phenols and carbazoles and diaromatics, which extend to the highest boiling ranges. The reaction 5 stoichiometric coefficient is fixed, $\gamma_{H_2, Da, i} = 3$. N-aromatics, O-N-aromatics and pyridines tend to disappear rapidly via reactions 7 – 9. They are complex mixtures and comprise mainly lighter compounds, up to C15. We assume that their final products are lost, as well as those of C8 phenol. Reaction 7 allows intermediate N-aromatics to be considered. The N- and O- fractions are respectively assumed to produce NH₃ and H₂O. The N- and O- content of carbazoles, phenols, N-aromatics, O- N-aromatics and pyridines has been adjusted to fit the elemental analysis. So, the NH₃ and H₂O stoichiometric coefficients are equal to the N- and O- mole content of the parent molecule per Eq. (3) and (4). The H₂ consumption stoichiometric coefficients account for the extra N- and O- content as shown in

Table 2. Where there are losses, the H₂ consumption stoichiometric coefficients are assumed and the losses stoichiometric coefficients are calculated to complete the mass balance.

$$\gamma_{NH_3,f,i} = x_{N,f,i} \quad (3)$$

$$\gamma_{H_2O,f,i} = x_{O,f,i} \quad (4)$$

The heavy, C₃₀₊ and CHO solid lumps shown in Figure 1 (c) are mixtures covering a wide boiling range and are assumed to produce mainly losses and gases via reactions 10 – 12. During model development, it was observed that CHO solid also appears to be a monoaromatics source. Solid N is well quantified and produces NH₃ via reaction 13, $\gamma_{H_2,N} = 1.5$. An average molar mass is assigned to each of the heavy, C₃₀₊ and CHO solid lumps and stoichiometric coefficient values for reactions 10 – 12 are unknown. For simplification, and to minimize the number of parameters for estimation, some assumptions are made regarding the stoichiometric coefficients, as shown in Table 2: one H₂ consumption stoichiometric coefficient is assumed for all the heavy lumps, one CH₄ production stoichiometric coefficient is assumed for the C₃₀₊, carbazoles and diaromatics and the ratio of C₂H₆ to CH₄ production is assumed to be the same for the solid and C₃₀₊ lumps. No CH₄ or C₂H₆ production was associated with C₃₀₊ amides.

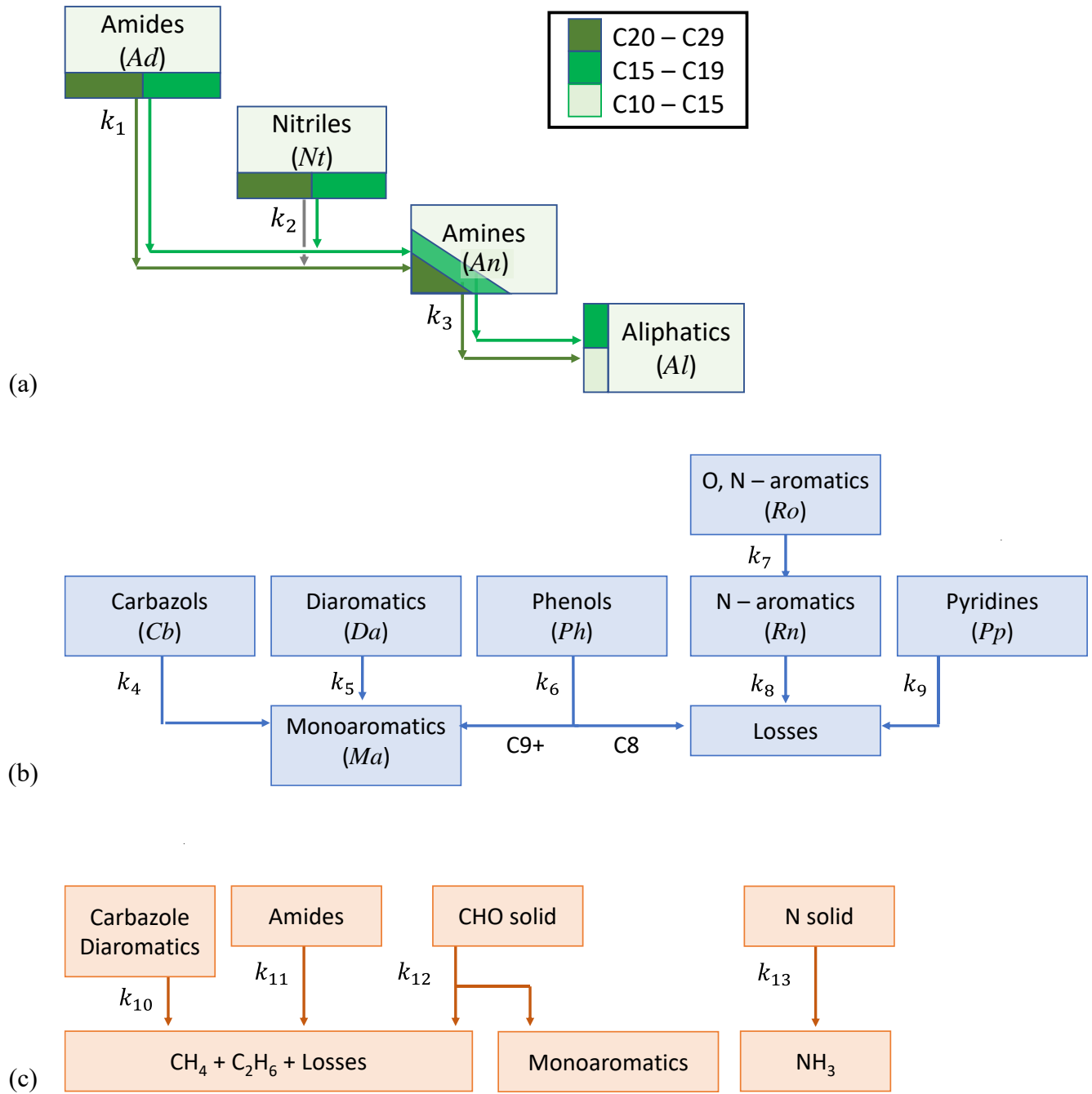


Figure 1. Optimised general reaction scheme with (a) straight chains, (b) aromatics and (c) heavy (C30+) and solid lumps.

Table 2. List of reactions, reaction rate equations and carbon number range.

	Reaction	Rate	Range
1	$Ad_i + \gamma_{H_2,Ad,i} H_2 \xrightarrow{k_1} An_i + H_2O$	$k_1 C_{Ad,i} C_{H_2}$	15 – 29
2	$Nt_i + \gamma_{H_2,Nt,i} H_2 \xrightarrow{k_2} An_i$	$k_2 C_{Nt,i} C_{H_2}$	15 – 29
3	$An_i + \gamma_{H_2,An,i} H_2 \xrightarrow{k_3} Al_i + NH_3$ $An_i + \gamma_{H_2,An,i} H_2 \xrightarrow{k_3} Al_j + Al_k + NH_3$	$k_3 C_{An,i} C_{H_2}$	15 – 19 20 – 29
4	$Cb_i + \gamma_{H_2,Cb,i} H_2 \xrightarrow{k_4} Ma_i + \gamma_{NH_3,Cb,i} NH_3 + \gamma_{H_2O,Cb,i} H_2O$	$k_4 C_{Cb,i} C_{H_2}$	11 – 29
5	$Da_i + \gamma_{H_2,Da,i} H_2 \xrightarrow{k_5} Ma_i$	$k_5 C_{Da,i} C_{H_2}$	11 – 29
6	$Ph_{C8} + \gamma_{H_2,Ph,C8} H_2 \xrightarrow{k_6} \gamma_{L,Ph,C8} L + \gamma_{H_2O,Ph,C8} H_2O$ $Ph_i + \gamma_{H_2,Ph,i} H_2 \xrightarrow{k_6} Ma_i + \gamma_{H_2O,Ph,i} H_2O$	$k_6 C_{Ph,i} C_{H_2}$	9 – 13 8
7	$Ro_i + \gamma_{H_2,Ro,i} H_2 \xrightarrow{k_7} Rn_i + \gamma_{H_2O,Ro,i} H_2O$	$k_7 C_{Ro,i} C_{H_2}$	9 – 15
8	$Rn_i + \gamma_{H_2,Rn,i} H_2 \xrightarrow{k_8} \gamma_{L,Rn,i} L + \gamma_{NH_3,Rn,i} NH_3$	$k_8 C_{Rn,i} C_{H_2}$	8 – 15
9	$Pp_i + \gamma_{H_2,Pp,i} H_2 \xrightarrow{k_9} \gamma_{L,Pp,i} L + \gamma_{NH_3,Pp,i} NH_3$ $+ \gamma_{H_2O,Pp,i} H_2O$	$k_9 C_{Pp,i} C_{H_2}$	8 – 15
10	$C30_f^+ + \gamma_{H_2,f,C30+} H_2 \xrightarrow{k_{10}} \gamma_{L,f,C30+} L + \gamma_{C30^+,CH_4} CH_4 +$ $\gamma_{\alpha} C_2H_6 + x_{N,C30+,f} NH_3 + \gamma_{H_2O,f,C30+} H_2O$	$k_{10} C_{Ph,i} C_{H_2}$	30+
11	$C30_{Ad}^+ + \gamma_{H_2,Ad,C30+} H_2 \xrightarrow{k_{11}} \gamma_{L,Ad,C30+} L$ $+ x_{N,C30+,Ad} NH_3 + \gamma_{H_2O,Ad,C30+} H_2O$	$k_{11} C_{Ph,i} C_{H_2}$	30+
12	$CHO_{(s)} + \gamma_{H_2,CHO} H_2 \xrightarrow{k_{12}} \gamma_{L,CHO} L + \gamma_{CH_4,CHO} CH_4 +$ $\gamma_{C_2H_6,CHO} C_2H_6 + \gamma_{Ma,CHO} Ma_{C10-C18}$	$k_{12} C_{Ph,i} C_{H_2}$	N/A
13	$N_{(s)} + \gamma_{H_2,N} H_2 \xrightarrow{k_{13}} NH_3$	$k_{13} C_{N(s)} C_{H_2}$	N/A

3.3 Parameter Estimation

The system of differential equations was resolved in MATLAB R2019b²⁰ using the solver `ode15i` and parameter estimation was carried out using MATLAB R2019b²⁰ non-linear least squares solver function, `lsqnonlin`, with the trust-region-reflective algorithm. This minimises an objective function based on an input vector of differences between measured and calculated data. Here, the differences were normalised to balance against overweighting the data points with greatest mass.

Parameter significance levels and confidence limits were determined from Eq.s (5) and (6)²¹. J is the Jacobian matrix and $se(b_p)$ is the standard error found for each parameter. SSE , n_d and p are the objective function and the numbers of data points and parameters respectively. b_p is the parameter value, t_{obs} is the observed student t-value. The parameter significance levels are found from the Student t-table. Eq. (7) is the formula for the correlation between parameters p and q . Parameter estimation was part of model development. So that only parameters of > 95% significance were included in the final version of the model.

$$se(b_p) = \sqrt{\frac{SSE ((J^T J)^{-1})_{pp}}{(n_d - p)}} \quad (5)$$

$$t_{obs} = \frac{b_p}{se(b_p)} \quad (6)$$

$$C_{p,q} = \frac{\{(J^T J)^{-1}\}_{p,q}}{\sqrt{\{(J^T J)^{-1}\}_{p,p} \{(J^T J)^{-1}\}_{q,q}}} \quad (7)$$

4. Results and Discussion

All pre-exponential factors at reference temperature and activation energies have been estimated excepted for the reactions 5, 7 to 9 and 13. These last being not sensitives to the temperature, only the overall kinetic constant k_r is given. The estimated parameters, all significant to $> 95\%$, are given in Table 3 along with their confidence limits. There is no correlation between $k_{r,350}$ for reactions 1 to 9 except, as expected, between $k_{r,350}$ and Ea_r for the same r . There is correlation between the C30+ and CHO- solid reaction rate constants, $k_{10,350}$ and $k_{12,350}$ and between the gas stoichiometric coefficients, γ_{13,CH_4} , γ_{C30+,CH_4} and γ_{13,C_2H_6} , indicating that the C30+ carbazoles and diaromatics and solid CHO-lump parameters are interrelated. Finally, two parameters related to monoaromatics sources have a correlation coefficient of 0.77: the diaromatics reaction rate constant, k_5 , and the solid CHO stoichiometric coefficient for monoaromatics production, $\gamma_{Ma,CHO}$. Both parameters are kept in the model since they are significant to $> 95\%$, to maintain the logic of the reaction scheme and to allow the model to produce sufficient monoaromatics.

Figure 2 compares the summed model outputs and measured data at reaction temperatures 350, 375 and 390°C for the four distributed families involved in straight chain reactions 1 – 3: amides, nitriles, aliphatic amines and aliphatics. The model gives a good fit for amides disappearance and aliphatics overall production rates as well as the nitriles and intermediate aliphatic amines, present in smaller quantity. From Table 3, the reaction 3 rate constant, $k_{3,350}$, is greater than those for reactions 1 and 2, $k_{1,350}$ and $k_{2,350}$, ensuring no accumulation of aliphatic amines. Reaction 1 and 2 activation energies, Ea_1 and Ea_2 , are

consistent with thermal activation, also visible in the evolution through reaction temperatures 350 – 390°C shown in Figure 2 (a) - (c).

Figure 3 gives the detail of the carbon number mass distributions for the amides and aliphatics at 350 and 390°C. The shift from the heavier amides to the lighter aliphatics distribution in the model is due to the assumption that C20 to C29 are secondary aliphatic amines, breaking into two halves in reaction 3. In general, the model fits the mass distributions well. However, there is a source of C14, C15 aliphatics which is not captured.

Table 3. Estimated parameters with confidence limits.

Reaction	$k_{r,350}$ (m ³ .mol ⁻¹ .h ⁻¹)	Ea_r (kJ.mol ⁻¹)
1 (Ad)	$1.93 \cdot 10^{-4} \pm 0.73 \cdot 10^{-4}$	174 ± 51
2 (Nt)	$1.32 \cdot 10^{-4} \pm 1.25 \cdot 10^{-4}$	212 ± 113
3 (An)	$1.30 \cdot 10^{-3} \pm 0.47 \cdot 10^{-3}$	137 ± 47
4 (Cb)	$1.67 \cdot 10^{-5} \pm 1.03 \cdot 10^{-5}$	398 ± 68
6 (Ph)	$5.60 \cdot 10^{-5} \pm 0.19 \cdot 10^{-5}$	96.8 ± 39.9
10 (Cb Da)	$4.73 \cdot 10^{-5} \pm 1.50 \cdot 10^{-5}$	306 ± 37
11 (Ad)	$3.25 \cdot 10^{-4} \pm 1.70 \cdot 10^{-4}$	233 ± 94
12 (CHO)	$5.95 \cdot 10^{-5} \pm 0.13 \cdot 10^{-5}$	73.5 ± 20.4
Reaction	k_r (m ³ .mol ⁻¹ .h ⁻¹)	
5 (Da)	$1.07 \cdot 10^{-4} \pm 0.26 \cdot 10^{-4}$	
7 (Ro)	$9.81 \cdot 10^{-4} \pm 0.25 \cdot 10^{-4}$	
8 (Rn)	$1.83 \cdot 10^{-3} \pm 0.35 \cdot 10^{-3}$	
9 (Pp)	$5.15 \cdot 10^{-4} \pm 1.56 \cdot 10^{-4}$	
13 (N)	$2.08 \cdot 10^{-4} \pm 0.32 \cdot 10^{-4}$	

Stoichiometric coefficient (-)	γ_{H_2}	γ_{CH_4}	$\gamma_{C_2H_6}$	γ_{Ma}
10 (Cb Da)	14.5 ± 2.8	6.10 ± 1.21	-	-
11 (Ad)		-	-	-
12 (CHO)		3.68 ± 0.73	4.51 ± 0.79	$9.29 \cdot 10^{-3} \pm 1.66 \cdot 10^{-3}$

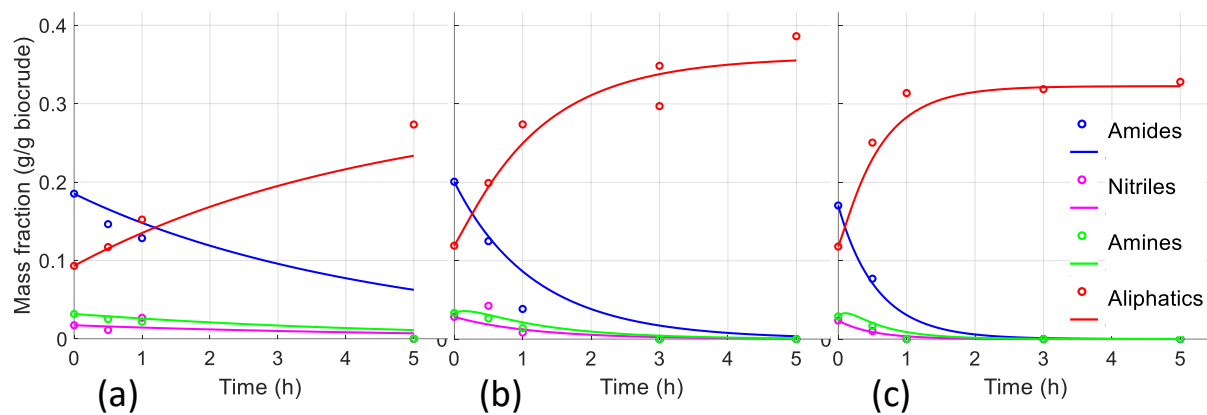


Figure 2. Comparison between calculated and measured overall mass fractions of straight chain families (a) 350°C, (b) 375°C and (c) 390°C.

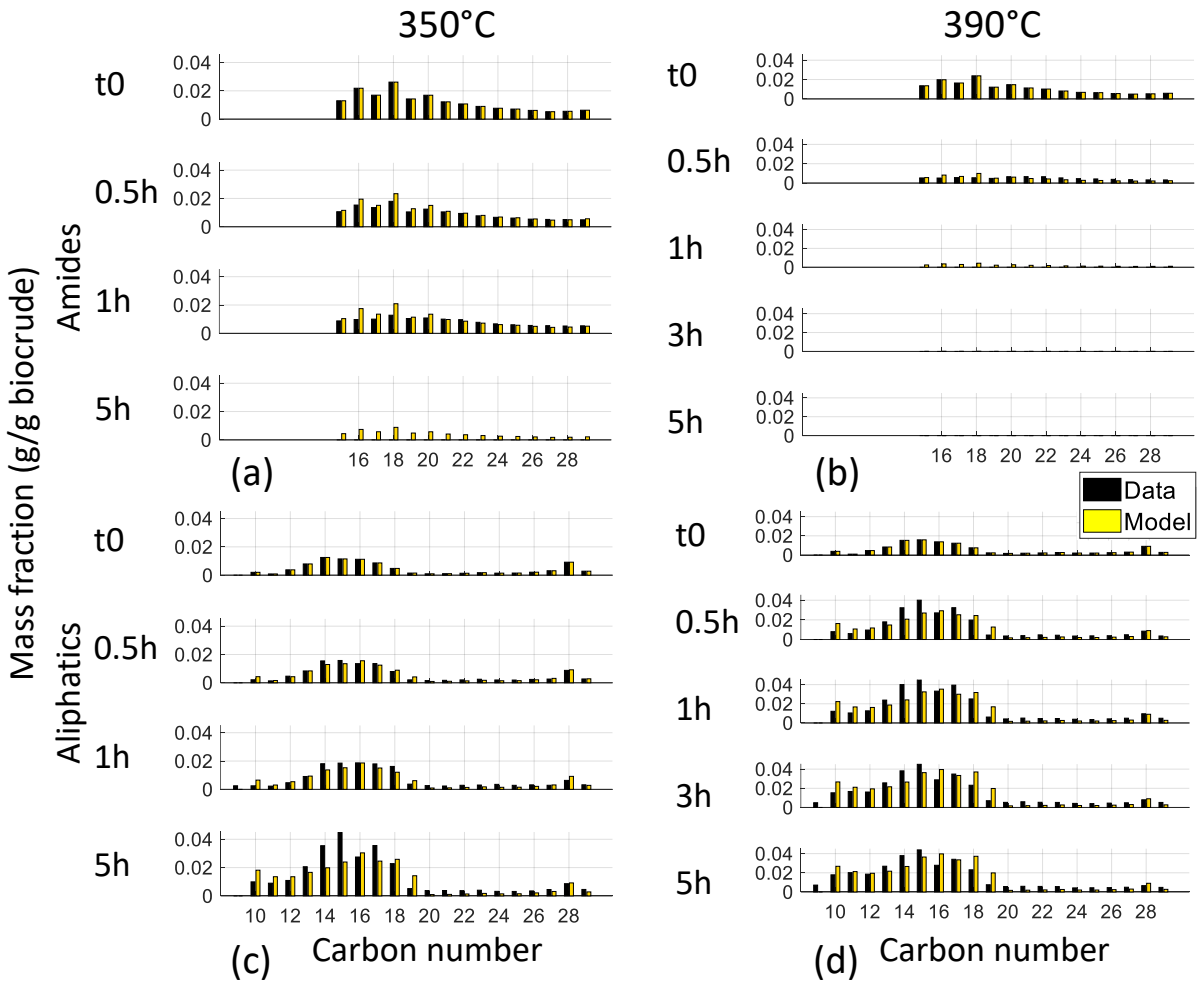


Figure 3. Comparison between calculated and measured mass fractions of (a) amides at 350°C, (b) amides at 390°C, (c) aliphatics at 350°C and (d) aliphatics at 390°C.

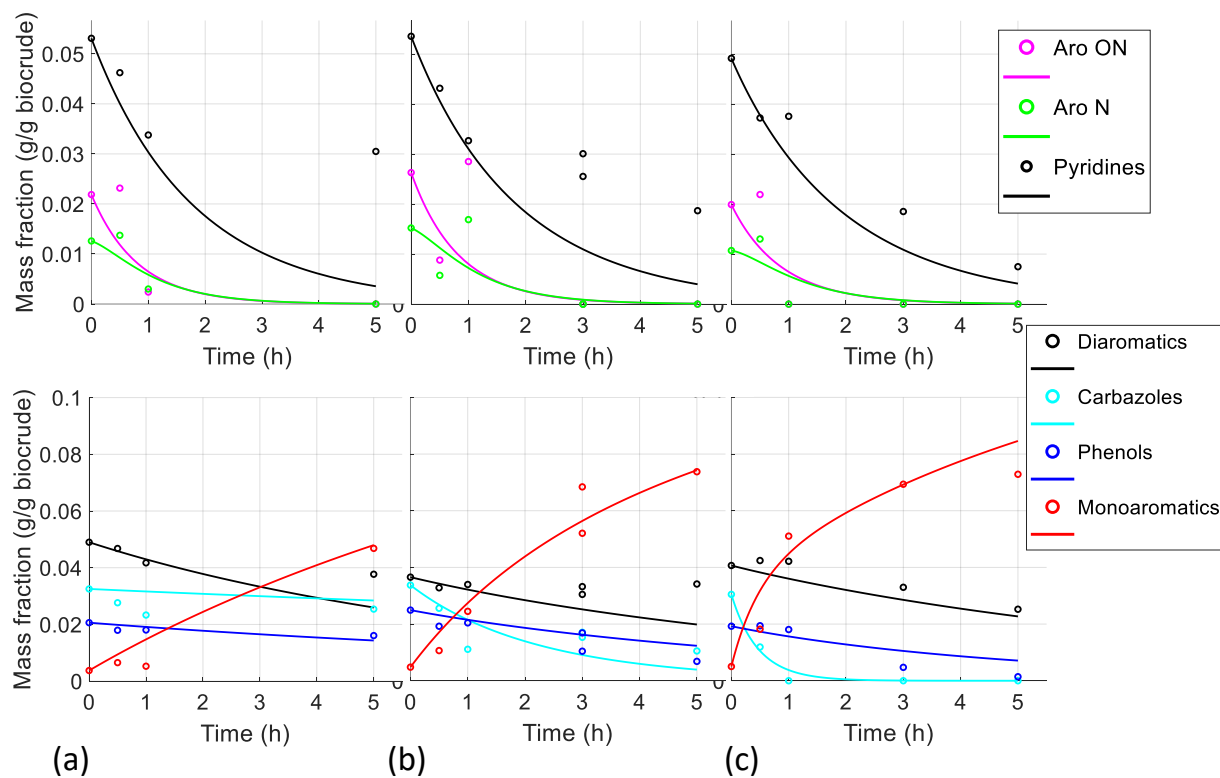


Figure 4 compares the overall model outputs and measured data at reaction temperatures 350, 375 and 390°C for the aromatic families. For the N-aromatics, O- N-aromatics, quantities are small, there are few, quite scattered data points and the model outputs approach the average evolution of the data points. The calculated pyridines, diaromatics and carbazoles outputs fit the 390°C experimental data with some discrepancies at lower temperature experiments. The phenols and monoaromatics model results are relatively good. The simplifying assumption of first-order reaction is quite approximative here. The N-aromatics, O- N-aromatics and pyridines are mixtures, so a higher reaction order might have given a better fit. Also, catalytic DN reactions are likely for N-aromatics, pyridines and carbazoles and, in this case, Langmuir-Hinshelwood kinetics taking account of active sites might be appropriate. However, the estimated 350°C reaction rate constants are consistent with the data. $k_{7,350}$, $k_{8,350}$ and $k_{9,350}$ for N-aromatics, O- N-aromatics and pyridines producing losses are all one or two magnitudes greater than $k_{4,350}$, $k_{5,350}$ and

$k_{6,350}$ for carbazoles, diaromatics and phenols giving monoaromatics. Only phenol and carbazole activation energies, Ea_6 and Ea_4 , are calculated. The increasing carbazole disappearance rate with temperature is clear from the data. However, the assumption of first-order reaction determines the shape of the curve for carbazoles disappearance and Ea_4 could be overestimated. Figure 5 shows the carbon number mass distributions for the sum of the liquid monoaromatics sources (diaromatics plus carbazoles and phenols) and the monoaromatics. The liquid monoaromatics sources disappear slowly and have a different profile to the monoaromatics products. Solid CHO is a fourth source of C10 to C18 monoaromatics, which allows the model to fit the monoaromatics profile. C10 to C18 is also the range of the aliphatic products and a reversible hydrogenation/dehydrogenation reaction between the monoaromatics and naphthenes probably exists. This reaction was tested by considering naphthenes separately but not found to be significant for this data set.

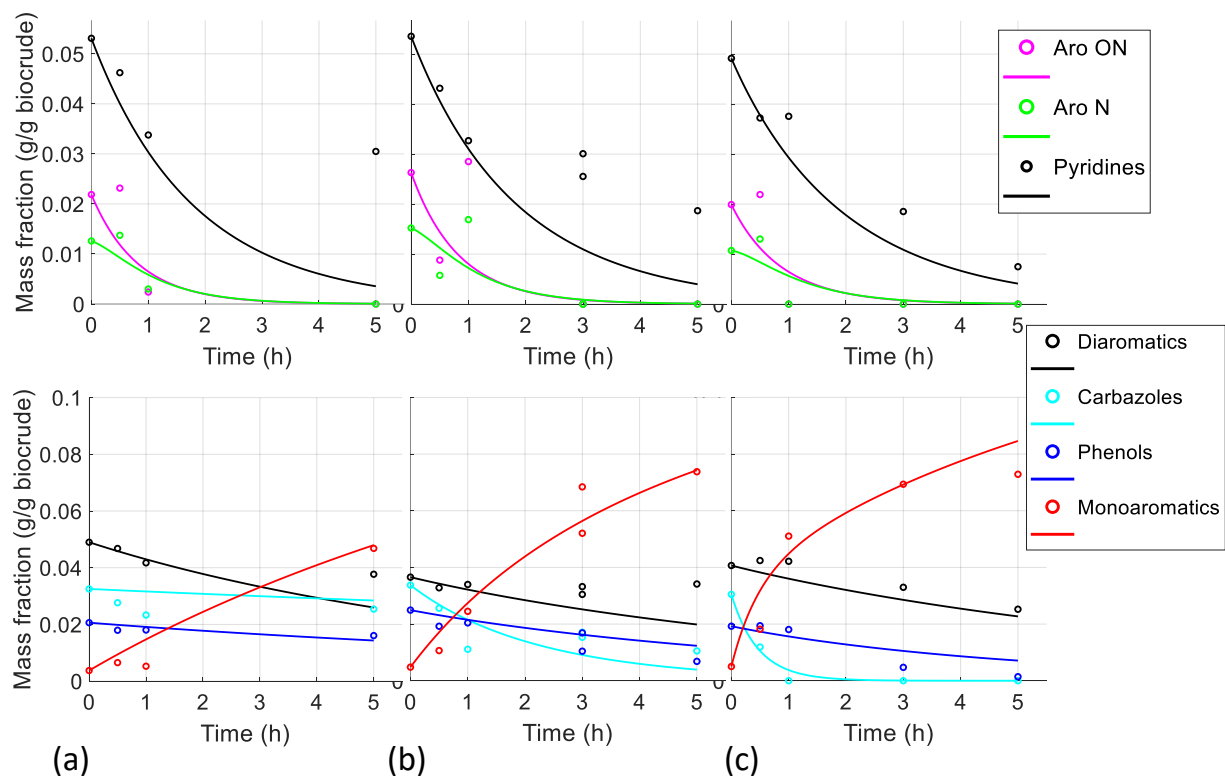


Figure 4. Comparison between calculated and measured overall mass fractions of aromatic families at (a) 350°C, (b) 375°C and (c) 390°C.

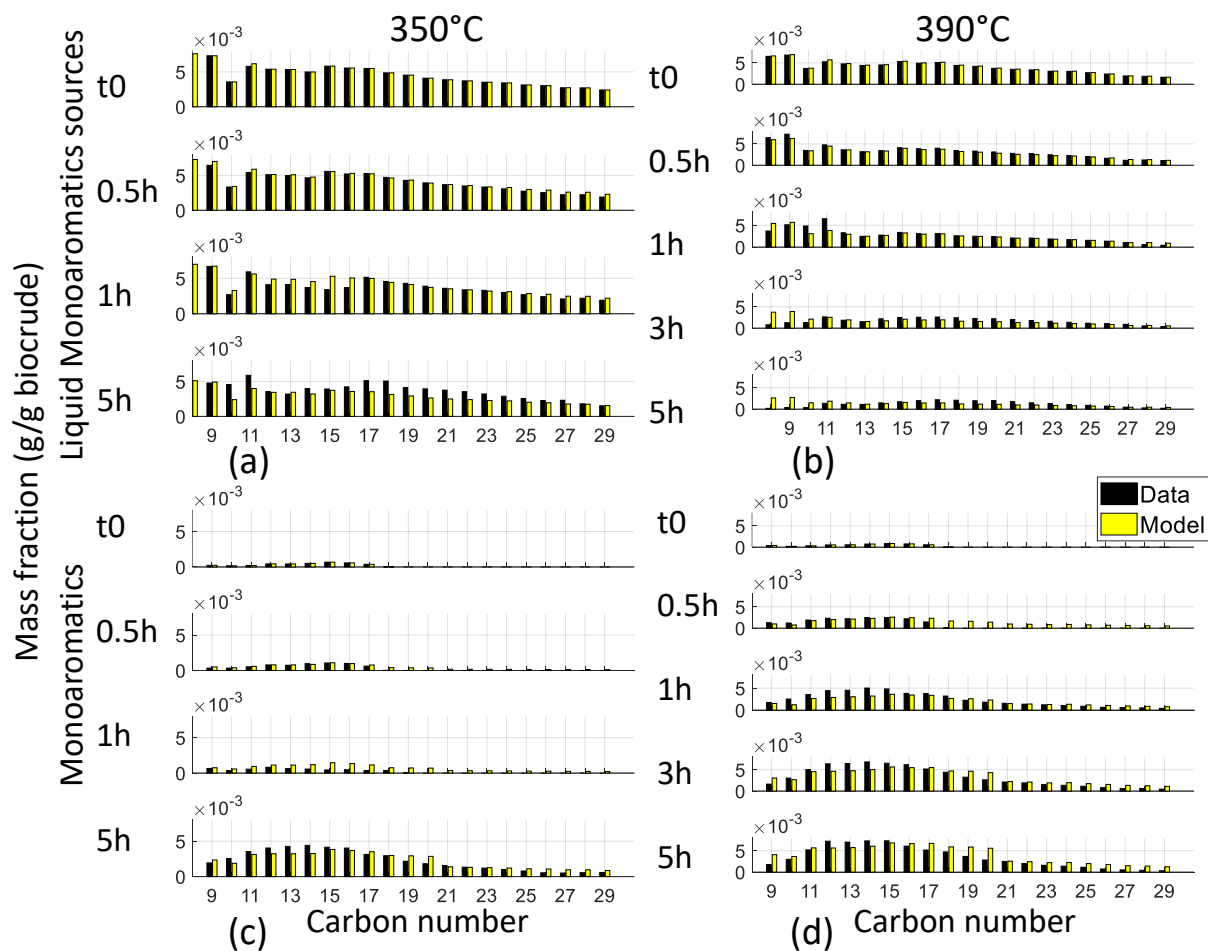


Figure 5. Comparison between calculated and measured mass fractions of (a) liquid monoaromatics sources at 350°C, (b) liquid monoaromatics sources at 390°C, (c) monoaromatics at 350°C and (d) monoaromatics at 390°C.

A comparison between calculated and measured solid N, solid CHO and reacting C30+ lumps is given in Figure 6. The model gives a good fit for all the available solids and most C30+ data points. From Table 3, the solid N reaction rate constant, k_{13} , is greater than that of solid CHO, $k_{12,350}$, at 350°C. The impact of the activation energy, Ea_{12} , is that both solid lumps have approximately the same reaction rate constant at 390°C.

The C30+ amides reaction rate constant, $k_{11,350}$, is greater than both that for the C30+ carbazoles and diaromatics and also the C15 – C29 amides reaction rate constant. This makes sense if the C30+ lump contains a greater fraction of tertiary amides, because tertiary amides are converted more rapidly than secondary amides due to the basicity of the amide group¹⁰ and could also provide the unidentified source of C14 and C15 aliphatics. Figure 6 illustrates the rapid disappearance of C30+ amides and includes the non-reacting C30+ aliphatics lump. We can see that there is very little variation in the C30+ aliphatics, and no increase which might correspond to C30+ amides products. This indicates that C30+ amides reactions are different to those for the C15 – C29 amides and justifies the choice to consider the C30+ amides separately.

Since the main area of interest of this study is in the boiling ranges where detailed information is available and the amount of C30+ carbazoles and diaromatics is relatively small, they are combined. The rate constant for the disappearance of the combined C30+ carbazoles and diaromatics, $k_{10,350}$, is logical, with a value between $k_{4,350}$ and $k_{5,350}$, for the C11 – C29 carbazoles and diaromatics respectively.

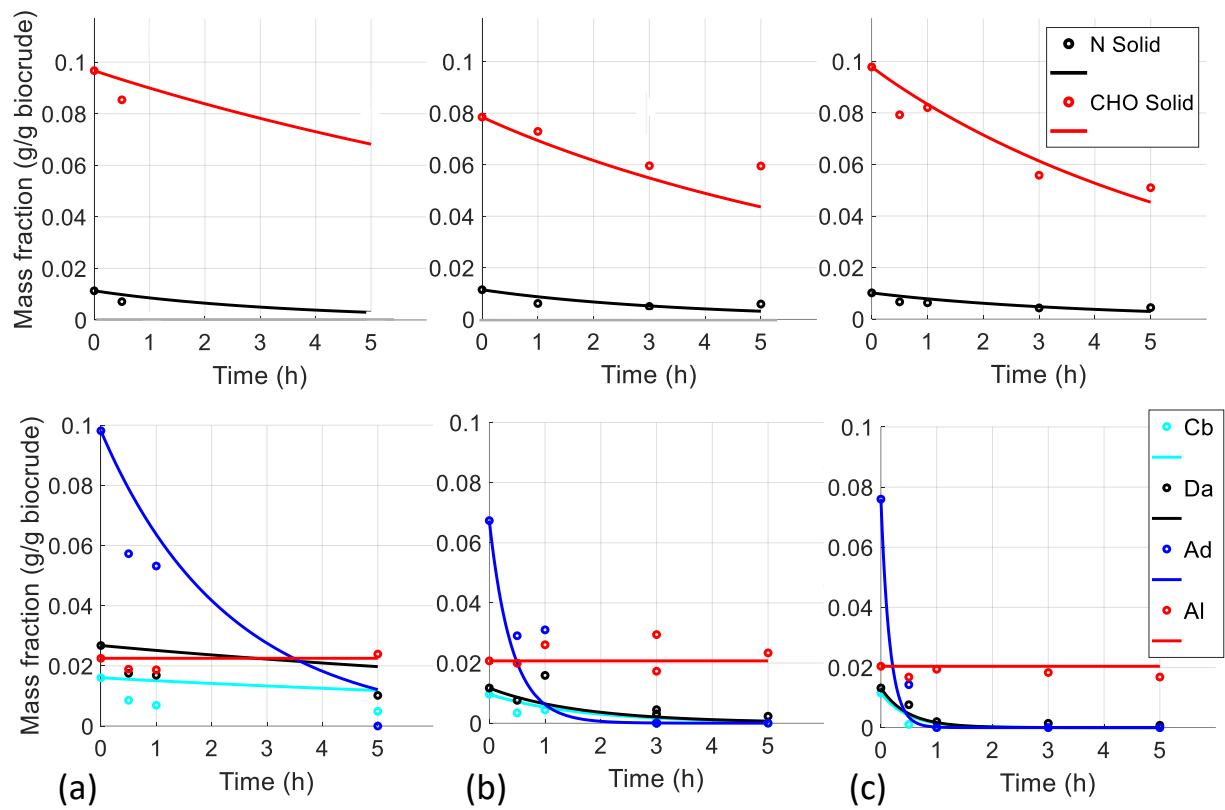


Figure 6. Comparison between calculated and measured overall mass fractions of solid and C30+ lumps at (a) 350°C, (b) 375°C and (c) 390°C.

Figure 7 compares model outputs to measured data for the gases. Figure 7 (a) shows that the model follows the H₂ consumption well at all three reaction temperatures. Figure 7 (b) considers losses and there is a discrepancy after 3 and 5h at 390°C. This discrepancy is possibly due to light hydrocarbons produced by hydrocracking and lost during the heptane evaporation stage. A hydrocracking reaction for aliphatics was considered but no significant reaction rate parameters were found. Indeed, hydrocracking could affect any of the families identified by GCxGC, so, the unaccounted for losses could be a general accumulation from several sources. Considering the discrepancy from a parameter estimation point of view: firstly, the applied weighting method was to divide the distance between measured and calculated data points by the measured data. So, the absolute size of the discrepancy is not relevant. Secondly, the residuals vector can be useful to identify where the parameter estimation is compensating for deficiencies in the model, such as a missing reaction. However, here, there are no correspondingly sized overestimates for the two or three data points representing the additional losses. In conclusion, the discrepancy seems to be due to a general effect.

Figure 7 (c) and (d) show that the model fits the data well for CH₄ and C₂H₆. Figure 7 (e) indicates that the model always overestimates the NH₃ production. In fact, the difference between total liquid N- content measured by elemental CHNO analysis and that calculated from the known functional groups increases with reaction time and temperature. So, the assumption that the N-compounds in the carbon number distributions have constant physical properties is not quite correct with respect to N- content, leading to this effect. The H₂O comparison in Figure 7 (f) has a better fit since O- content is much lower than N- content at the end of the reaction period.

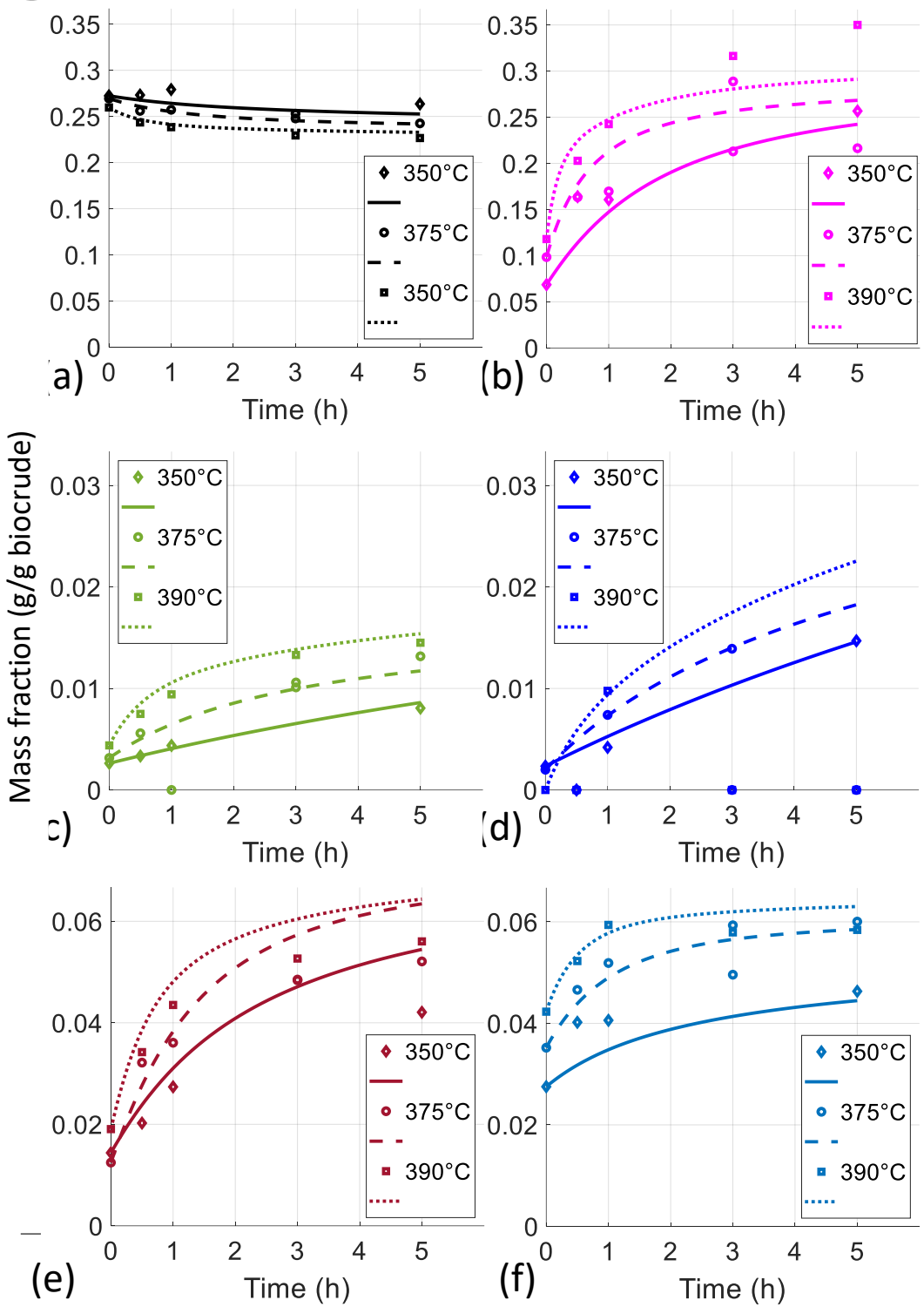


Figure 7. Comparison between calculated and measured overall mass fractions for (a) H₂, (b) Losses, (c) CH₄, (d) C₂H₆, (e) NH₃ and (f) H₂O.

5. Conclusion

A kinetic model based on laboratory scale upgrading of 3g HTL biocrude in a batch reactor with hydrotreatment catalyst has been constructed and analysed. The model has thirteen reactions and includes straight chains, aromatics and C30+ and solids. Reactions consume H₂ and produce H₂O and/or NH₃ depending on their functional groups. 26 parameters have been estimated in total: 13 reaction rate constants, 9 activation energies and 5 stoichiometric coefficients.

First-order reaction rate equations and the assumption that C15 – C19 aliphatic amines are primary whilst C20 – C29 aliphatic amines are secondary allow the model to fit the straight chain components well. The model output dynamics relative to the aromatics data points suggest higher order reactions for N-aromatics, O- N-aromatics and pyridines and, possibly, Langmuir Hinshelwood kinetics for N-aromatics, pyridines and carbazoles. This fits with the knowledge that the N-aromatics, O- N-aromatics and pyridines are mixtures of chemical structures and N-aromatics, pyridines and carbazoles tend to undergo catalytic reactions on active sites. However, the fit is relatively good. An additional source of monoaromatics was required and using the solid CHO reaction for this allowed the model to fit the data.

Two main discrepancies between the model and the data are in the NH₃ production rate and the losses production rate after 3 and 5 h at 390°C. These differences point to N accumulation in the liquid N-compounds during the reaction and a small amount of generalised hydrocracking at 390°C.

Acknowledgements

The authors would like to thank the European Commission Research Fund for Coal and Steel for supporting the HYCON project (Grant agreement number 899471).

Browning, Barbara; Batalha, Nuno; Costa Gomes, Margarida; Laurenti, Dorothee; Lebaz, Noureddine; Geantet, Christophe; Tayakout-Fayolle, Mélaz. Hydrotreatment of Sewage Sludge Derived Hydrothermal Liquefaction Biocrude. Part I: Experimental. *Energy & Fuels*. Manuscript ID: ef-2024-00883v.R2.” Accepted on 06 May 2024.

- (1) Mishra, R. K.; Kumar, V.; Kumar, P.; Mohanty, K. Hydrothermal Liquefaction of Biomass for Bio-Crude Production: A Review on Feedstocks, Chemical Compositions, Operating Parameters, Reaction Kinetics, Techno-Economic Study, and Life Cycle Assessment. *Fuel* **2022**, *316*, 123377. <https://doi.org/10.1016/j.fuel.2022.123377>.
- (2) Batalha, N.; Checa, R.; Lorentz, C.; Afanasiev, P.; Stańczyk, K.; Kapusta, K.; Laurenti, D.; Geantet, C. Lignite and Biomass Waste Hydrothermal Liquefaction Crude Upgrading by Hydrotreatment. *Energy Fuels* **2023**, *37* (14), 10506–10520. <https://doi.org/10.1021/acs.energyfuels.3c01550>.
- (3) Jensen, C. U.; Hoffmann, J.; Rosendahl, L. A. Co-Processing Potential of HTL Bio-Crude at Petroleum Refineries. Part 2: A Parametric Hydrotreating Study. *Fuel* **2016**, *165*, 536–543. <https://doi.org/10.1016/j.fuel.2015.08.047>.
- (4) Fan, Y.; Hornung, U.; Dahmen, N. Hydrothermal Liquefaction of Sewage Sludge for Biofuel Application: A Review on Fundamentals, Current Challenges and Strategies. *Biomass and Bioenergy* **2022**, *165*, 106570. <https://doi.org/10.1016/j.biombioe.2022.106570>.
- (5) Zimmermann, J.; Chiaberge, S.; Iversen, S. B.; Raffelt, K.; Dahmen, N. Sequential Extraction and Characterization of Nitrogen Compounds after Hydrothermal Liquefaction of Sewage Sludge. *Energy Fuels* **2022**, *36* (23), 14292–14303. <https://doi.org/10.1021/acs.energyfuels.2c02622>.
- (6) Jahromi, H.; Rahman, T.; Roy, P.; Adhikari, S. Hydrotreatment of Solvent-Extracted Biocrude from Hydrothermal Liquefaction of Municipal Sewage Sludge. *Energy Conversion and Management* **2022**, *263*, 115719. <https://doi.org/10.1016/j.enconman.2022.115719>.
- (7) Heracleous, E.; Vassou, M.; Lappas, A. A.; Rodriguez, J. K.; Chiaberge, S.; Bianchi, D. Understanding the Upgrading of Sewage Sludge-Derived Hydrothermal Liquefaction Biocrude via Advanced Characterization. *Energy Fuels* **2022**, *36* (19), 12010–12020. <https://doi.org/10.1021/acs.energyfuels.2c01746>.
- (8) Mederos, F. S.; Elizalde, I.; Ancheyta, J. Steady-State and Dynamic Reactor Models for Hydrotreatment of Oil Fractions: A Review. *Catalysis Reviews* **2009**, *51* (4), 485–607. <https://doi.org/10.1080/01614940903048612>.
- (9) Chehadeh, D.; Ma, X.; Al Bazzaz, H. Recent Progress in Hydrotreating Kinetics and Modeling of Heavy Oil and Residue: A Review. *Fuel* **2023**, *334*, 126404. <https://doi.org/10.1016/j.fuel.2022.126404>.
- (10) Zhu, C.; Gutiérrez, O. Y.; Santosa, D. M.; Flake, M.; Weindl, R.; Kutnyakov, I.; Shi, H.; Wang, H. Kinetics of Nitrogen-, Oxygen- and Sulfur-Containing Compounds Hydrotreating

- during Co-Processing of Bio-Crude with Petroleum Stream. *Applied Catalysis B: Environmental* **2022**, *307*, 121197. <https://doi.org/10.1016/j.apcatb.2022.121197>.
- (11) Jitumoni, B.; Dixit, S. A.; Pradeep, P. R.; Ravindra, K.; Das, S. K.; Christopher, J.; Sau, M.; Kapur, G. S.; Ramakumar, S. S. V. Study of Thermal Cracking Kinetics and Co-Processing of Biocrude in Thermal Residual Upgradation Unit for Converting ‘Waste to Energy.’ *J Therm Anal Calorim* **2023**, *148* (9), 3439–3456. <https://doi.org/10.1007/s10973-023-11941-8>.
 - (12) Jiang, H.; Sun, X.; Lv, H.; Chen, W.; Qin, K.; Li, M.; Nie, H. Hydrodenitrogenation Kinetics of Diesel Oil and Catalyst Stacking Simulation. *Energy Fuels* **2021**, *35* (4), 3283–3294. <https://doi.org/10.1021/acs.energyfuels.0c03502>.
 - (13) Pu, J.; Laurenti, D.; Geantet, C.; Tayakout-Fayolle, M.; Pitault, I. Kinetic Modeling of Lignin Catalytic Hydroconversion in a Semi-Batch Reactor. *Chemical Engineering Journal* **2020**, *386*, 122067. <https://doi.org/10.1016/j.cej.2019.122067>.
 - (14) Srinivas, B. K.; Pant, K. K.; Gupta, S. K.; Saraf, D. N.; Choudhury, I. R.; Sau, M. A Carbon-Number Lump Based Model for Simulation of Industrial Hydrotreaters: Vacuum Gas Oil (VGO). *Chemical Engineering Journal* **2019**, *358*, 504–519. <https://doi.org/10.1016/j.cej.2018.10.019>.
 - (15) Browning, B.; Afanasiev, P.; Pitault, I.; Couenne, F.; Tayakout-Fayolle, M. Detailed Kinetic Modelling of Vacuum Gas Oil Hydrocracking Using Bifunctional Catalyst: A Distribution Approach. *Chemical Engineering Journal* **2016**, *284*, 270–284. <https://doi.org/10.1016/j.cej.2015.08.126>.
 - (16) Browning, B.; Pitault, I.; Couenne, F.; Jansen, T.; Lacroix, M.; Alvarez, P.; Tayakout-Fayolle, M. Distributed Lump Kinetic Modeling for Slurry Phase Vacuum Residue Hydroconversion. *Chemical Engineering Journal* **2019**, *377*, 119811. <https://doi.org/10.1016/j.cej.2018.08.197>.
 - (17) Fang, X.; Shi, Y.; Wu, K.; Liang, J.; Wu, Y.; Yang, M. Upgrading of Palmitic Acid over MOF Catalysts in Supercritical Fluid of N-Hexane. *RSC Adv.* **2017**, *7* (64), 40581–40590. <https://doi.org/10.1039/C7RA07239B>.
 - (18) Xu, C.; Hamilton, S.; Mallik, A.; Ghosh, M. Upgrading of Athabasca Vacuum Tower Bottoms (VTB) in Supercritical Hydrocarbon Solvents with Activated Carbon-Supported Metallic Catalysts. *Energy Fuels* **2007**, *21* (6), 3490–3498. <https://doi.org/10.1021/ef700459s>.
 - (19) Wan, H.; Chaudhari, R. V.; Subramaniam, B. Catalytic Hydroprocessing of P-Cresol: Metal, Solvent and Mass-Transfer Effects. *Top Catal* **2012**, *55* (3–4), 129–139. <https://doi.org/10.1007/s11244-012-9782-6>.
 - (20) MATLAB R2019b.
 - (21) Rasmuson, A.; Andersson, B.; Olsson, L.; Andersson, R. *Mathematical Modeling in Chemical Engineering*; Cambridge University Press, 2014.